Forecasting **Products**

Research and Development

Forecasting Research
Technical Report No. 265

Development of a mountain wave turbulence prediction scheme for civil aviation

by

J. Turner

April 1999

The Met.Office

Excelling *in weather services*

Forecasting Research
Technical Report No. 265

Development of a mountain wave turbulence prediction scheme for civil aviation

by

J. Turner

April 1999

Aviation Applications Group
Room R321
Meteorological Office
London Road
Bracknell
Berkshire
RG12 2SZ
United Kingdom

Tel: 44 (0)1344 856245 Fax: 44 (0)1344 854026 e-mail: rwlunnon@meto.gov.uk

Abstract

The occurrence of turbulence to aircraft in-flight, is an increasingly expensive and sometimes dangerous hazard to civil aviation. As one of two World Area Forecast Centres, the UK Met. Office has a responsibility to forecast significant weather globally for international civil air traffic, including forecasts of Clear Air Turbulence (CAT). One of the main causes of CAT is the effects of mountains on low level flow, which can lead to breaking waves at cruising altitudes, and may be responsible for up to 30% of all turbulence encounters over land areas. An objective, global scheme for predicting mountain wave induced turbulence is required, which may be used as an operational tool in the production of turbulence forecasts to aviation customers.

This report documents the development of a scheme by which mountain wave turbulence events can be forecast objectively, using parameters from the Unified Model. Selected diagnostics from the gravity wave drag parameterisation, were tested in a regression analysis against an extensive dataset of turbulence and null reports from commercial aircraft. It was found that a combination of gravity wave stress fields displayed skill in prediction of turbulence events, comparable to that of the shear-induced CAT prediction methods currently in use. The use of upper tropospheric wind fields to represent effects downstream of orographic wave activity showed a further improvement in the skill.

The algorithm was tested and monitored in an operational context during a winter trial period, utilising both objective verification and input from aviation forecasters. The verification results further supported the skill found previously and the involvement of aviation forecasters proved successful in the specification of a product for operational use. This work ends with a recommendation for the implementation of a 'first guess' mountain wave turbulence forecasting tool, to be used to enhance current forecasts of CAT hazard areas on significant weather chart products.

Development of a mountain wave turbulence prediction scheme for civil aviation

1 Introduction

1.1 Background to aviation turbulence forecasting

In-flight turbulence encounters can be a dangerous and costly hazard to commercial airlines. The sudden changes of speed and altitude associated with such events can cause injury to passengers and crew and in some cases damage to the aircraft. Unlike convection-induced or 'cloudy' turbulence, clear air turbulence (CAT) has no visual warning signs, and cannot be detected ahead by current aircraft sensor technology. Clearly, accurate forecasts of turbulence risk areas at the flight planning stage are vital for minimising the risk of the most dangerous encounters on commercial air routes. As one of two World Area Forecasting Centres (WAFCs), the UK Meteorological Office has a responsibility to provide forecasts of upper air significant weather, including CAT, to international flight planners and ICAO[1]. These are currently in the form of significant weather (SIGWX) charts, where turbulence risk areas are indicated along with associated height and severity.

There are two principle sources of CAT at cruising altitudes: wind shear and mountain waves. Wind shear induced CAT can be predicted with some skill as it is typically associated with jets, where the horizontal and vertical wind shears are high. A 'first guess' prediction scheme is included in the Met. Office's Unified Model (UM) which indicates areas of likely hazard due to this type of turbulence, and is used in global aviation forecasting. This is then enhanced manually by the forecaster.

Mountain wave induced CAT arises from the instability caused by breaking gravity waves, which are induced at low levels by the presence of orography. If the low level flow is such that air is forced to rise over hills or mountains, gravity wave energy is propagated upwards through the atmosphere, transporting momentum to higher levels. Wave breaking and hence turbulence often occurs around the upper troposphere, at typical cruising altitudes. At present, no objective predictor of mountain wave turbulence (MWT) is available to forecasters and it is typically under-forecast.

CAT is typically a highly localised phenomenon, both temporally and spatially. A number of independent studies have been made to understand and model the mechanisms behind gravity wave breaking, and these have often utilised high resolution local models (e.g. Heimann, 1997; Doyle *et al.*, 1998). Since the physical scale of gravity waves is typically a few kilometres, their effects must be represented by parameterisations in lower resolution and global models.

This report describes the development of an objective 'first guess' global prediction algorithm, suitable for operational use alongside the existing shear induced turbulence predictor, to enhance CAT forecasts on SIGWX charts. As with the shear CAT scheme, it is required that the scheme uses global model diagnostics.

It should be noted that although both shear-induced turbulence and MWT are known as forms of clear air turbulence, both may occur in when cloud is present. In contrast convective turbulence is a direct result of up-draughts and motions within clouds, particularly large convective systems.

---

[1] ICAO: International Civil Aviation Organisation

1.2 Preliminary work and case study

Prior to the work described in this report, preliminary studies were made to identify the most suitable model parameters for use as inputs to a prediction algorithm. The UM gravity wave drag parameterisation diagnostics were identified as those most relevant for MWT prediction. Both gravity wave stress and drag (due to the deposition of stress) were investigated as potential inputs to a MWT prediction algorithm.

Initial global plots of gravity wave stress showed a relationship with mid-latitude westerlies, particularly in winter, and the presence of mountain ranges oriented perpendicular to the prevailing wind direction. A case study of the Alps was undertaken, in which gravity wave stress fields were compared with aircraft reports of turbulence for a number of contrasting synoptic situations. Although the data used were limited, there was a strong correlation between gravity wave stress in the upper troposphere and turbulence reports from aircraft at these altitudes over the Alps (Turner, 1997).

Building on these results, the following sections of this report describe the development of a global algorithm suitable for operational use. Chapter 2 describes the requirements of such a product in the context of the current WAFC products. Chapter 3 gives a brief summary of the parameterisation used in the UM and the derivation of the gravity wave diagnostics. Chapter 4 describes the statistical methods used to investigate the skill of their use in a global MWT predictor. Finally chapter 5 details an operational trial of a developmental algorithm to define a useful product for WAFC forecasters. The report concludes in chapter 6 with a recommendation for the product to be implemented along with suggestions for additional work for future enhancement of the product.

2 The WAFC forecasting requirement

WAFC London, based at the UK Met. Office is one of two WAFCs, which are required to provide global meteorological information for use by airlines and international organisations for flight planning purposes. As well as providing global forecasts of winds and temperatures for use in fuel and time calculations, forecasts of significant meteorological features and hazards are required for route planning.

Significant weather (SIGWX) charts covering specified areas are routinely produced showing the positions of features which affect aircraft in-flight. The main set of charts produced for global coverage is concerned with altitudes above 25,000 ft (FL250). Currently six chart areas are routinely produced by WAFC London, but both WAFCs must have the capability to provide forecasts for any region of the globe (see Murray and Olson, 1999). In general, the Pacific region is covered by WAFC Washington.

Each set of SIGWX charts are produced by two forecasters four times daily and distributed by fax to ICAO. The charts are valid at a single time per set: 0Z, 6Z, 12Z and 18Z. They are produced using data from the twice-daily global model run, and need to reach the customers at least 12 hours ahead of their valid time. Hence, forecast model data used has a lead-time of either 18 or 24 hours.

2.1 Chart description

Relevant charts are provided in hard copy format to the pilots of all international commercial flights, and detail relevant meteorological information for the flight (figure 1.1). Their purpose is to mark the positions and strengths of jet streams and highlight areas of hazard such as turbulence. The features plotted on the chart are:

- Jets (position, height and wind speed)
- Tropopause heights, including maxima and minima
- CAT areas (maximum of 12), with heights and severity for each area
- Convective cloud, with heights
- Active volcano locations
- Hurricanes
- Positions of surface fronts, with arrows indicating direction of movement

The dashed areas indicate regions where moderate or severe turbulence is likely. The heights and turbulence severity relating to each enclosed area are marked in a key at the bottom of the chart, where there is provision for only 12 areas to be referenced. Hence, small fragmented CAT areas are not favoured and there is a tendency to forecast larger areas to include small pockets. Therefore over-forecasting CAT areas is a problem with this constraint.

2.2 Current CAT prediction methods

The 'first guess' for the position and severity of CAT risk locations is provided directly from the UM, but only addresses shear-induced CAT. The field displays contours indicating the probability of a turbulence encounter (maximum 7%). Heights are derived

empirically from wind shear calculations made by the forecaster. Enhancement to the objective field is made by the forecaster to correct the first guess e.g. increasing CAT severity where the jet shows strong curvature, and reducing it for the strongest jets where flow is smooth. The skill of this predictor and a comparison with alternative methods is documented in Bysouth (1998).

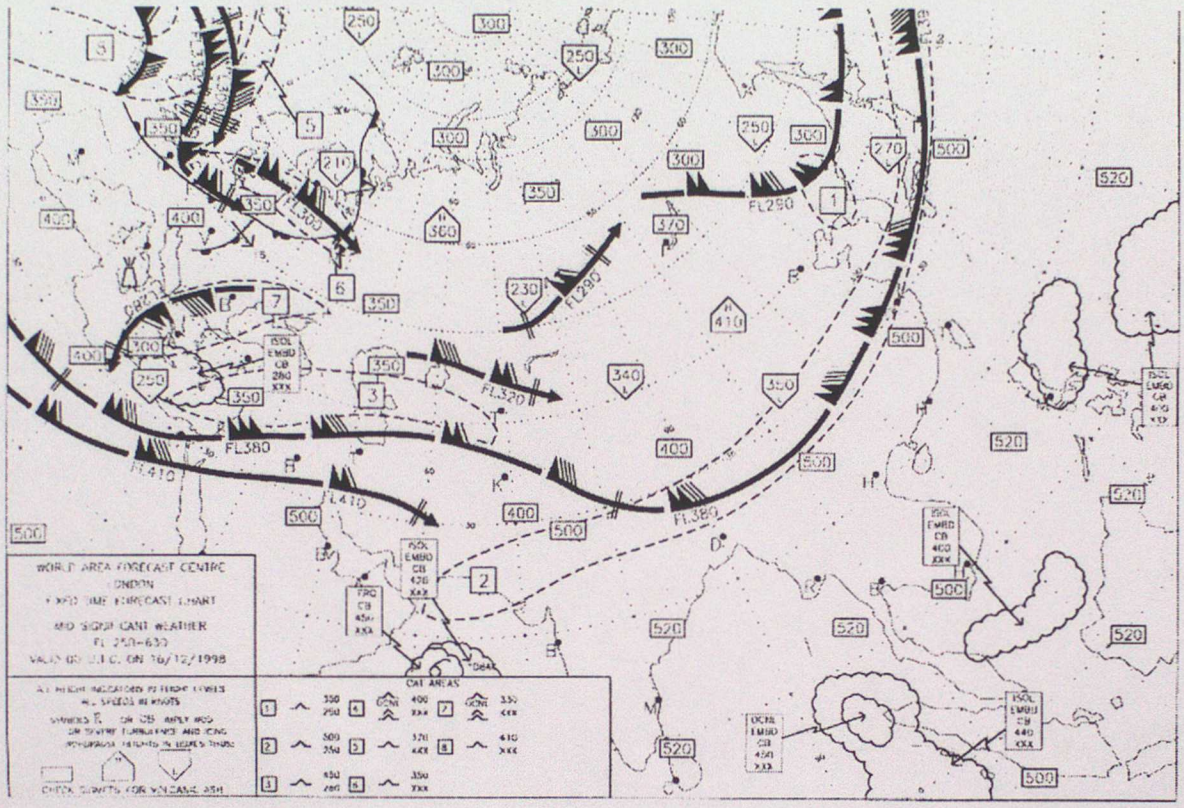

Figure 1.1: *Example of Significant weather chart produced for FL250-650, showing jets, tropopause heights, convective cloud and CAT areas. Fronts are also marked*

Currently, there are no objective tools for predicting MWT and it is only marked in its own right due to the experience and intuition of the forecaster. Section 6.1.2 of the Forecasters Reference Book describes the conditions under which MWT events are most likely. All of these require consideration of the surface or low level flow. Thus, for a forecaster to add mountain wave CAT areas to the SIGWX chart, they would necessarily have to spend time combining various sources of information (e.g. surface wind fields, stability and satellite images) for each area of concern. Clearly, when a number of chart areas are to be done, this process would take considerable time as it has to be repeated for each region where the forecaster suspects mountain wave activity to be a hazard.

2.3 MWT forecast requirements

This report describes the development of a first guess global prediction algorithm, suitable for use alongside the existing shear induced turbulence predictor, to enhance the CAT forecasts on the SIGWX charts. This would complete the objective capability for turbulence forecasting and allow MWT to be forecast in the same way as shear induced CAT, eliminating the need for time-consuming derivation. This would in turn facilitate increased value in forecasts of CAT from all sources with no loss in efficiency.

Although on the final SIGWX product, there is no distinction between the physical causes of each marked CAT area, the algorithm would be treated in the chart production process

as a separate forecast field to the existing predictor. This is necessary to avoid confusion between the sources of turbulence. The forecasters' intervention is a necessary part of the process and requires knowledge of how the model has diagnosed turbulence regions. Since in many cases, areas of MWT may overlap areas of diagnosed shear turbulence due to the coincidence of the contributory factors, a mountain wave algorithm would be treated as an enhancement tool, secondary to the shear CAT field.

The skill in predicting shear-induced CAT is limited largely by the finite vertical resolution of the model, since vertical wind shear and its representation is a major factor in prediction skill. It is expected that the prediction of MWT will be less dependent on vertical resolution as on the horizontal gridscale of the model, since gravity waves are a parameterised feature. The aim is to develop an algorithm which displays comparable skill in prediction of wave induced turbulence to the method used operationally to produce the shear CAT 'first guess' field.

Since turbulence in all its forms is characteristically very localised both temporally and spatially, the aim here is not to pinpoint individual turbulence events, but to find an algorithm, which consistently defines areas within which a defined probability of a turbulence encounter is true. Statistical methods are used to define and verify this requirement.

An objective prediction tool based on global model forecast fields from the UM could be combined with existing or improved shear CAT algorithms and potentially be used for future forecast products requiring a greater degree of automation (see Murray, 1999). The global coverage would also provide capability to apply the scheme to any required region of the world. This work could ultimately contribute to further automation of such forecast products in the future.

3 The gravity wave drag scheme in the UM

3.1 Introduction

Details of the theory of gravity wave turbulence may be found in the extensive literature on the subject (e.g. Shutts, 1998; Kim and Mahrt, 1992). In summary, gravity wave stress is propagated upwards from its source at the surface, hence transporting momentum vertically. As the air density decreases, and the wind changes direction with height, the maximum stress which can be sustained is reduced, and the excess is deposited by wave breaking. This deposition of momentum induces local instability, and gives rise to turbulence in the mid and upper troposphere. Since the surface stress is induced by low level flow being disrupted by the presence of orography, this wave-breaking phenomenon occurs above mountainous regions.

The purpose of the orographic gravity wave drag scheme in the UM is to adjust the tropospheric and lower stratospheric wind fields to maintain the global momentum budget. The 'breaking' of gravity waves applies a drag effect, decelerating the wind fields throughout the troposphere and stratosphere. Over orography, the stresses associated with these waves can be one or two orders of magnitude greater than those of a turbulent boundary layer (Kim and Mahrt, 1992) and may be considered the principle mechanism for drag effects over mid-latitude land masses. Since the gravity waves themselves are smaller than the gridscale of the global model (around 60km) these effects are parameterised. The scheme uses orographic variability data and combinations of wind and stability diagnostics to diagnose the initial surface stress, which is then used to calculate the vertical stress profile and hence drag.

Improvements to the parameterisation scheme, including better representation of orography and improved mechanisms of orographic forcing, were proposed, tested (Milton *et al.*, 1994), and were subsequently implemented into the operational model in 1996. This more accurate parameterisation better represents the physics of gravity wave stress production and processes leading to wave breaking and hence turbulence. Although the parameterisation scheme only accounts for vertical transport of the stress, there are documented cases of turbulence effects tens of kilometres downstream from the source (e.g. Tilley et al., 1998). This effect is important in a turbulence forecasting context.

The remainder of this chapter outlines the parameterisation scheme and highlights some of the approximations and assumptions made in it. This is intended only as an aid to understanding the capabilities and limitations of the scheme in the context of its use in turbulence prediction. Full documentation is available from the Physical Parameterisation Group, Hadley Centre. Details of the global model are available from the UKMO.

3.2 Parameterisation description

The surface stress at each gridpoint is calculated first. Then for each point the corresponding vertical stress profile is then determined, taking into account a number of conditions leading to stress deposition and hence wave breaking. These include low level blocking, lee waves and hydraulic jump and saturation stress.

3.2.1 Model specifics and grid considerations

The parameterisation aims to represent gravity waves of the scale of a few kilometres, much less than the current gridscale of the global forecasting model (around 60km for mid-latitudes). Future increases in resolution may approach the wavelength of the larger scale waves, whose effects will then be represented physically. The gravity wave stress is calculated for each gridpoint at all model half-levels. Each complete horizontal grid of values is referred to as a model 'field'. If stress deposition is diagnosed at a particular gridpoint and level, the associated drag or deceleration, $\partial u/\partial t$ is applied at that point due to the stress, τ, according to the relationship

$$\frac{\partial u}{\partial t} = g\frac{\partial \tau}{\partial p} \qquad (1)$$

Where $\partial\tau$ is represented by the stress difference between the half-levels immediately above and below the full level on which the drag is calculated. Similarly, ∂p is represented by the pressure difference between these levels. The drag field is output on full model levels.

The parameterisation scheme requires a number of model fields as inputs. These are:

- Orography ancillary fields
- Surface pressure field, P*
- U and V components of wind
- Potential temperature, θ, for stability calculation

The potential temperature, pressure and orography fields are calculated on a global grid of 432 x 325 points, known as the P-grid. The stress and drag fields, along with the wind fields, to which they are applied, are calculated on a 432 x 324-staggered grid, known as the U-grid. Before any calculations are made, the wind fields are linearly interpolated onto the P-grid, on which all the computations are performed and the resulting stress and drag fields are then interpolated back onto the U-grid, to enable correction of the wind field due to orographic drag. Therefore, the stress field output from the model is already interpolated, and as such is a smoothed version of the actual parameterised stress. This should be borne in mind when considering extreme or point values.

3.1.2 Surface stress calculation

The first stage of the calculation is to determine the surface stress at all grid points. This is the starting point for calculation of the vertical profile for each point. The calculation is only performed for land points, with all sea points automatically assigned zero values. Typically, surface stress is also zero for a small proportion of land points.

Ancillary orography fields are used in the surface stress calculation. Fields are derived from the standard deviation of orography for each gridbox, calculated from a 10-minute global orography dataset produced by the US Navy. This representation of orographic variability gives a measure of the 'abruptness' of height changes and hence the effects on the low level flow encountering topographic peaks within the gridbox. This variance is also represented in perpendicular x and y directions separately, representing the directional orographic variation. The fields used, symbolised by σ_{xx}, σ_{yy} and σ_{xy} are known as the *anisotropic orography* fields.

The use of anisotropic orography allows the orographic variance to be calculated in u and v components and is then easily related to wind direction and the surface stress vector. It then follows that the wind direction relative to that of the ridge has a strong influence on the magnitude of the surface stress, and in turn on the stress and drag profiles aloft.

The x and y surface stress components, denoted by τ_{sx} and τ_{sy} are calculated as follows:

$$\tau_{sx} = \rho K^{-1} C\left[\sigma_{xx} \cos\chi + \sigma_{xy} \sin\chi\right]$$

$$\tau_{sy} = \rho K^{-1} C\left[\sigma_{xy} \cos\chi + \sigma_{yy} \sin\chi\right]$$

where K is a scaling constant and C is a function of the Brunt Vaïsala frequency (N), orographic variance (σ) and wind speed in the x or y direction. χ denotes the angle of the wind vector relative to the westerly direction and ρ is the density. The point to note is that if a strong wind in statically stable conditions encounters a ridge perpendicular to the flow, the surface stress will be high, and in a direction perpendicular to the orientation of the ridge.

The surface stress at each point is then scaled by a transmission factor, which accounts for reflection of internal gravity wave energy within the atmosphere. In cases of high winds and stability, a blocking situation at low levels may be diagnosed.

3.1.3 Vertical stress profile

There are several conditions which characterise the vertical stress profile, given a non-zero surface stress value. Each gridpoint position is considered separately, and stress values are passed upwards to the corresponding gridpoint in the next vertical layer, and so each 'column' is effectively treated in isolation. There is no horizontal transfer of momentum and no advection of gravity wave effects.

In the absence of conditions, which satisfy criteria for one of the stress deposition mechanisms, the total stress from a point is transferred vertically to the next level in the column. However, if either a hydraulic jump, a critical level or saturation stress is diagnosed, some or all of the remaining stress is deposited within that layer, leaving a reduced stress value for the next level. This is then translated into a deceleration according to the relationship (1). The three principle mechanisms are as follows:

Hydraulic jump points: The scheme tests the low-level wind and stability conditions to find those points for which low-level wave breaking is diagnosed. In this case, a proportion of the total surface stress in that column is deposited linearly up to a hydraulic jump height, H_c. This height is dependent on the vertical wavelength, a function of wind speed in the direction of the stress and the buoyancy frequency, N. The vertical stress profile up to H_c for this regime is shown in figure 3.1a.

Critical layers: In the case of a 1-dimensional orographic ridge, the direction of the stress vector would lie in a direction perpendicular to the ridge. The 'effective wind' is that component of the wind vector which is parallel to the stress vector. If the actual wind remains in a similar direction to the stress vector as height increases, then the majority of the stress will be propagated upwards to the next level. However, if the wind direction turns through 90°, whereby there is no longer a component in the direction of surface stress vector, all the stress must be deposited below this level. In the case of a hydraulic jump point, the surface stress is deposited linearly with height from the surface up to this critical level (figure 1.3b).

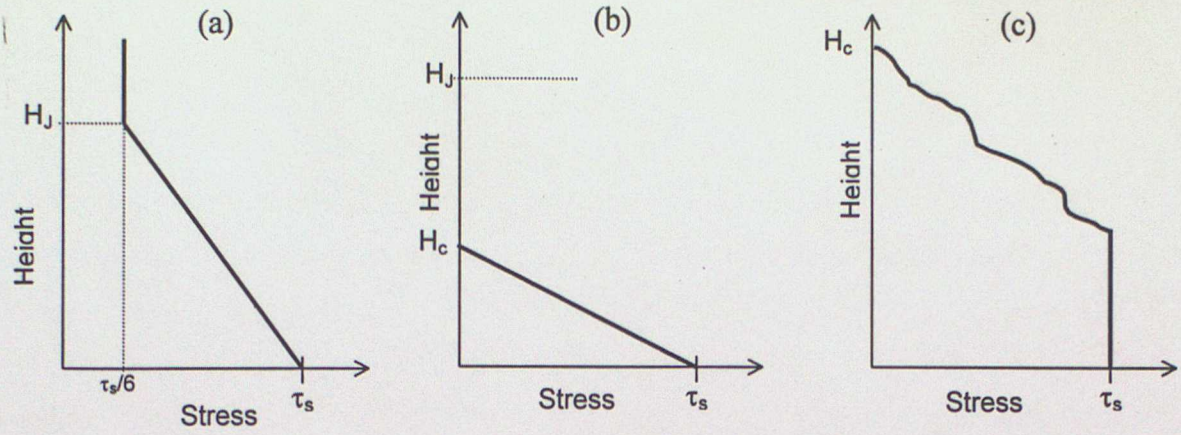

Figure 1.3 Column profiles of gravity wave stress under different regimes: a) Hydraulic jump, where 5/6 of the original surface stress is deposited up to the jump level; b) Critical level occurring below hydraulic jump point, where all stress is deposited linearly; c) Saturation regime where excess stress is deposited at each level for which the critical value is exceeded, until a critical level is reached.

Saturated stress deposition: Above a hydraulic jump point, or in columns where a hydraulic jump is not diagnosed, the surface stress is propagated upwards through the column, and is only deposited when the critical saturation stress value at that level is exceeded. This is dependent on the wind speed and direction of at each level, the density and the static stability. As the air density decreases in each layer, the critical stress reduces with height and the stress passed upwards from the lower layers will eventually exceed the maximum sustainable value. The excess is then deposited as drag, according to the relationship (1). This continues for each level in the column until a critical layer is reached, whereby all the stress is deposited in the layer immediately below it (figure 3.1c). This regime also applies for the remaining stress in the column above a hydraulic jump level.

Lee wave drag: At low levels, lee waves also lead to stress deposition and hence modification of the vertical profile. This will not be detailed here, as the effects are largely confined to lower levels, and thus do not directly affect the problem of upper tropospheric turbulence forecasting.

3.2 Output gravity wave fields

The output fields from the scheme consist of the stress components in the U and V directions and a number of acceleration or drag fields, all interpolated onto the U-grid.

Separate fields are output for acceleration due to hydraulic jump, lee waves, and saturation stress. However, no single gridpoint at a given level will have non-zero drag values for both hydraulic jump and saturation stress, since only one or the other of the mechanisms applies to each point. Typical global fields of both stress and drag are shown in figure 3.2.

Magnitudes of stress over particularly active areas may be as high as 1 or 2 Pa, but more typically, values fall in the range 10^{-5} - 0.1 Pa. Many land points have smaller or zero stress values. This field may be considered as an indicator of the most likely areas at risk from turbulence, by highlighting the most active gravity wave sources. However, actual wave breaking is only diagnosed by the model at points where the drag fields are non-zero.

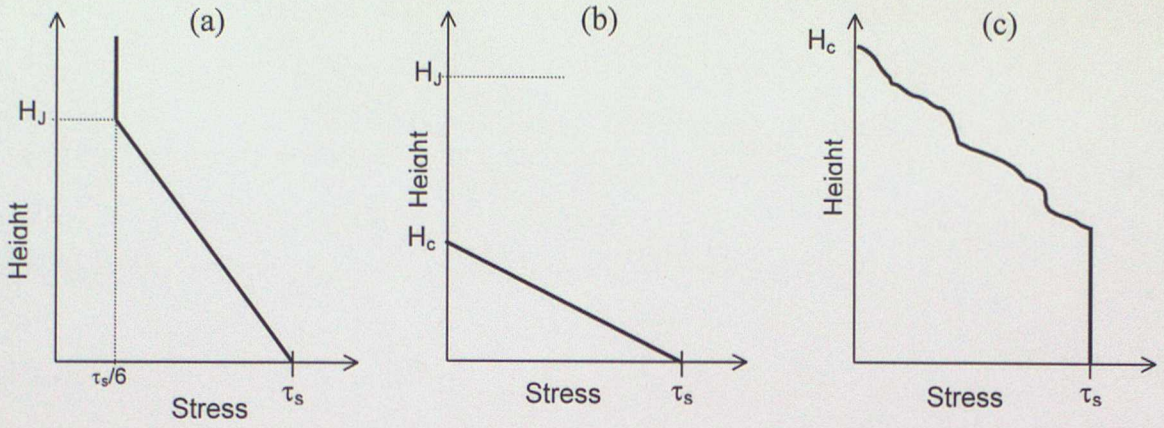

Figure 1.3 *Column profiles of gravity wave stress under different regimes:* ***a)*** *Hydraulic jump, where 5/6 of the original surface stress is deposited up to the jump level;* ***b)*** *Critical level occurring below hydraulic jump point, where all stress is deposited linearly;* ***c)*** *Saturation regime where excess stress is deposited at each level for which the critical value is exceeded, until a critical level is reached.*

Saturated stress deposition: Above a hydraulic jump point, or in columns where a hydraulic jump is not diagnosed, the surface stress is propagated upwards through the column, and is only deposited when the critical saturation stress value at that level is exceeded. This is dependent on the wind speed and direction of at each level, the density and the static stability. As the air density decreases in each layer, the critical stress reduces with height and the stress passed upwards from the lower layers will eventually exceed the maximum sustainable value. The excess is then deposited as drag, according to the relationship (1). This continues for each level in the column until a critical layer is reached, whereby all the stress is deposited in the layer immediately below it (figure 3.1c). This regime also applies for the remaining stress in the column above a hydraulic jump level.

Lee wave drag: At low levels, lee waves also lead to stress deposition and hence modification of the vertical profile. This will not be detailed here, as the effects are largely confined to lower levels, and thus do not directly affect the problem of upper tropospheric turbulence forecasting.

3.2 Output gravity wave fields

The output fields from the scheme consist of the stress components in the U and V directions and a number of acceleration or drag fields, all interpolated onto the U-grid.

Separate fields are output for acceleration due to hydraulic jump, lee waves, and saturation stress. However, no single gridpoint at a given level will have non-zero drag values for both hydraulic jump and saturation stress, since only one or the other of the mechanisms applies to each point. Typical global fields of both stress and drag are shown in figure 3.2.

Magnitudes of stress over particularly active areas may be as high as 1 or 2 Pa, but more typically, values fall in the range 10^{-5} - 0.1 Pa. Many land points have smaller or zero stress values. This field may be considered as an indicator of the most likely areas at risk from turbulence, by highlighting the most active gravity wave sources. However, actual wave breaking is only diagnosed by the model at points where the drag fields are non-zero.

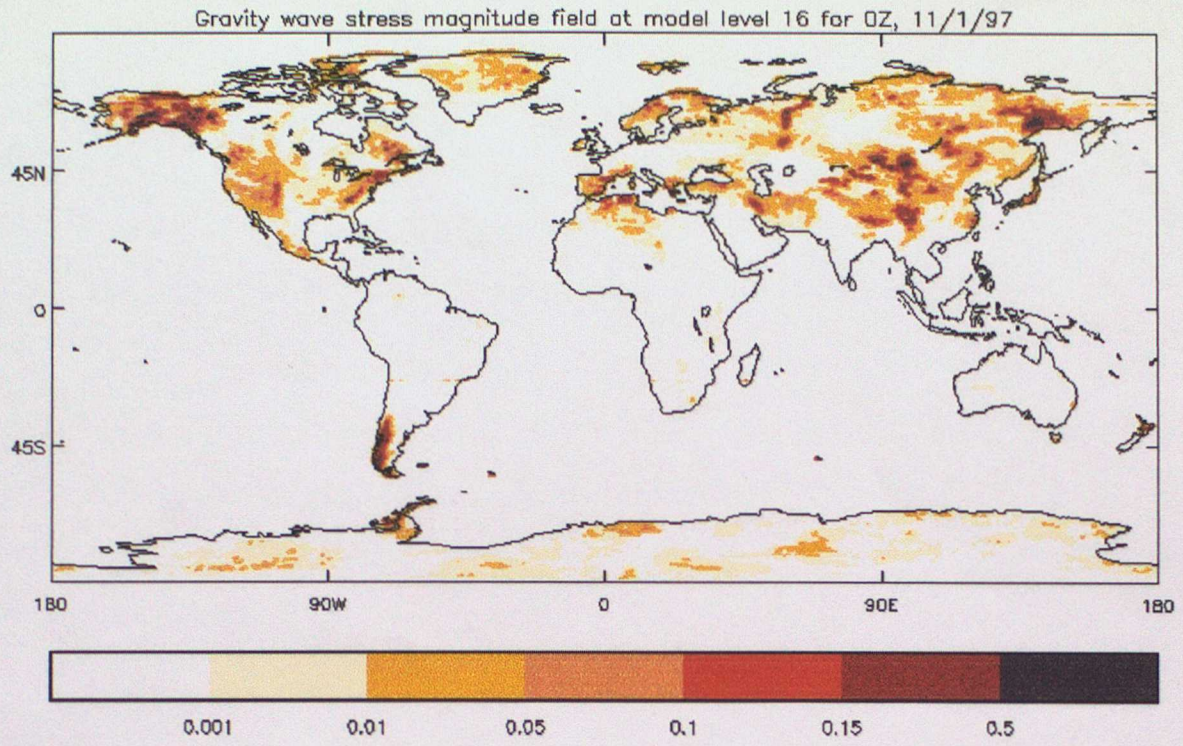

b)

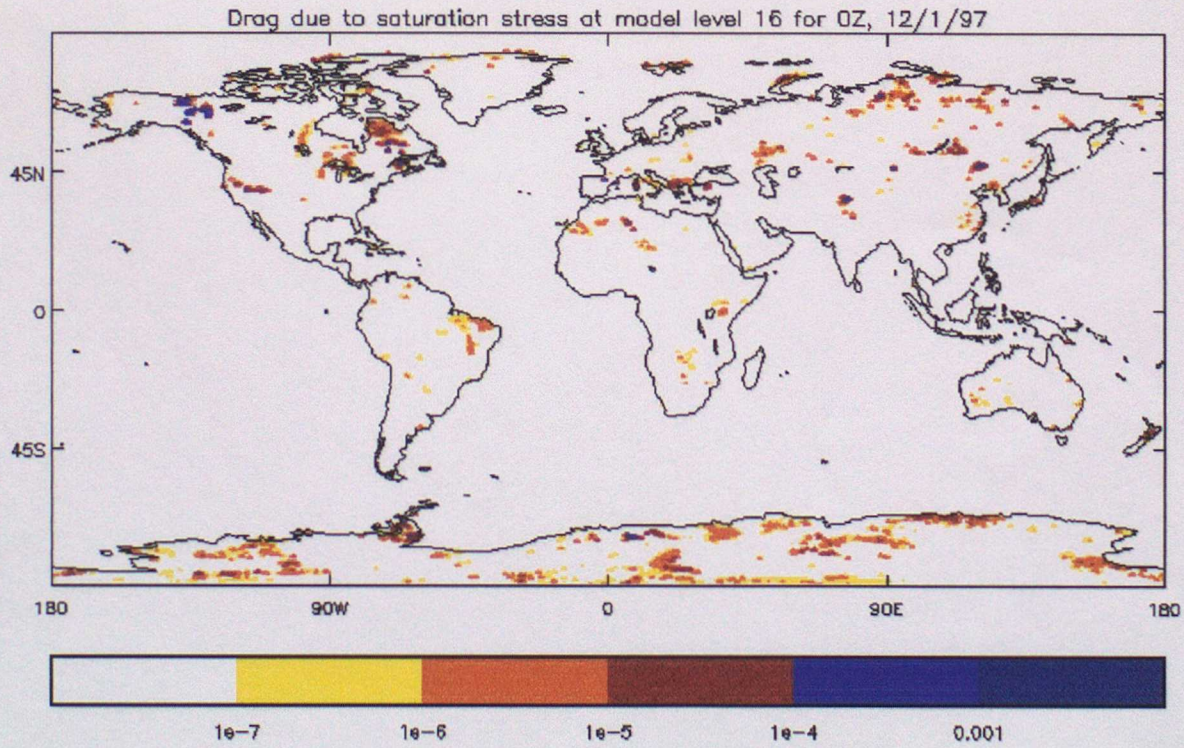

Figure 3.2 a) *global plot of a typical gravity wave stress field at approx. 28,000 ft.* ***b)*** *typical plot of drag field for the same height. Note the more fragmented characteristic of the drag field, compared with the stress field.*

Acceleration or drag values are typically around 10^{-2} ms^{-2} in active regions and less than 10^{-5} otherwise. There are many zero values in any given field, either due to complete stress deposition lower in the column, or the critical saturation stress not being exceeded. Although these fields should indicate points at which breaking waves and hence turbulence occurs. However, it gives a much less broad indication of the gravity wave activity in general.

3.3 The gravity wave scheme in a MWT forecasting context

This chapter has summarised the theory and parameterisation of breaking gravity waves in the context of its use in a turbulence predictor. The scheme takes into account the surface conditions necessary to give rise to orographic gravity waves and includes calculations of wind and static stability throughout the column to diagnose the likely levels at which wave breaking and therefore turbulence is likely to occur. This reasoning follows the guidelines published in the Forecasters' Reference Book on diagnosing MWT. Hence use of these output fields should show some skill at indicating MWT areas globally, and a forecast product based on this therefore has potential to aid the enhancement of operational CAT forecasts, with minimal extra overhead.

Although shear-induced CAT and MWT are separately considered, there are conditions which may arise, where both conditions occur concurrently and forecasters should be aware of these. For example, if a jet crosses an area of high gravity wave activity, the high wind speeds may enhance the breaking wave effects diagnosed by the model, and thus show an area of CAT due to both effects. In reality this may correspond to more severe event, as both mechanisms may combine in an additive way. For example, if a jet crosses a mountain range at angle perpendicular to the surface stress vector, it may cause all the remaining stress below that level to be deposited, giving rise to wave breaking and turbulence.

Although trapped lee waves are associated with air lifting over orography in stable conditions, the organised wave patterns, which are seen on satellite imagery, do not necessarily correspond to areas of likely turbulence. Rather, it is the disorganised overturning effect, which characterises the hazard.

4 Global algorithm development

4.1 Introduction

From the analysis of the gravity wave drag parameterisation and the results of the case study performed for the Alps, there is strong indication that UM diagnostics can be used in forecasting MWT. Since the requirement for WAFC products is to have global capability, a more extensive study was required using global data to assess whether one or more gravity wave parameters could be combined to produce a global mountain wave CAT predictor. This chapter describes the use of global model fields and aircraft reports to develop a prediction algorithm to indicate for MWT hazard areas.

Within areas where conditions are conducive to CAT, actual occurrences are often short-lived and extremely localised. As such it is unrealistic to attempt to provide a definitive forecast of individual events. Instead, the aim is to identify and flag areas within which the probability of encountering moderate or severe turbulence exceeds a given threshold. Although the model fields used in this study are derived from a physical parameterisation of the effects of orographic wave activity, the methods used in this study are statistical, and lead to a solution based on statistical results.

In this investigation, a large volume of aircraft data and corresponding UM fields of gravity wave stress and drag were needed, with data covering as much as possible of the main continental land areas. These were required for a continuous trial period, ideally over a number of weeks, to enable a regression analysis on a suitably large sample of data.

4.2 Model data

4.2.1 High resolution three week dataset

In the previous small-scale case studies, gravity wave fields were obtained by re-running the UM for the appropriate days, since they were not operationally available. For the more extensive global study, a number of fields from each day were required for around a 20 day period, making this impractical in terms of time and computing costs. In addition, the new high-resolution global grid became operational in early 1998 and so it was desirable to use fields of this new resolution to be representative of future operational model output. Since maximum mountain wave activity occurs in the northern hemisphere winter, the trial would have maximum benefit if data from this period were used.

To satisfy these issues, gravity wave stress and drag fields were requested as outputs from a three-week pre-implementation trial of the new high-resolution global grid, using data valid for January 1997. These fields had a horizontal grid of 432 x 325 points, giving a mid-latitude resolution of approximately 60km, and 30 vertical levels, increased from 19 in the previous operational version (see Milton *et al.*, 1998).

A total of 90 fields valid at 0Z for each day were obtained, representing a continuous 21 day period from 3-23 January 1997 (see table 4.1). For operational WAFC products, T+18 and T+24 fields are used since around a 12-hour lead-time is required by the customer, once the products have been dispatched. The use of T+12 fields in this study was a compromise between being representing this lead-time, and minimising errors in the forecast fields, in order to show a clearer relationship between the model parameterisation and 'truth' data.

Field name	Levels	Data time	Valid time
Gravity wave stress (U component)	10 – 23 (half levels)	12Z T+12 2 – 22 January 1997	0Z 3 – 23 January 1997
Gravity wave stress (V component)	10 – 23 (half levels)	12Z T+12 2 – 22 January 1997	0Z 3 – 23 January 1997
U-Acceleration due to saturated stress	10 – 23 (full levels)	12Z T+12 2 – 22 January 1997	0Z 3 – 23 January 1997
V-Acceleration due to saturated stress	10 – 23 (full levels)	12Z T+12 2 – 22 January 1997	0Z 3 – 23 January 1997
U-Acceleration due to hydraulic jump	10 – 23 (full levels)	12Z T+12 2 – 22 January 1997	0Z 3 – 23 January 1997
U-Acceleration due to hydraulic jump	10 – 23 (full levels)	12Z T+12 2 – 22 January 1997	0Z 3 – 23 January 1997
Wind (U component)	200, 250, 300 hPa (standard levels)	12Z T+12 2 – 22 January 1997	0Z 3 – 23 January 1997
Wind (V component)	200, 250, 300 hPa (standard levels)	12Z T+12 2 – 22 January 1997	0Z 3 – 23 January 1997

***Table 4.1**: Global fields used in the global algorithm development process*

4.2.2 Gravity wave fields

Two fields at each level were derived from the model fields obtained for each day of the trial and used as independent regression variables in the algorithm development. These were derived as follows:

Gravity wave stress: although this does not diagnose breaking waves, it gives a broad indication of gravity wave activity over orography. The gravity wave stress field used was a magnitude calculated from the U and V component fields. This provided a single continuous variable representing the 'potential for wave breaking' within a gridbox.

Gravity wave acceleration (drag): the acceleration fields have non-zero values at points where momentum is being deposited due either to hydraulic jump or saturation stress being exceeded. At any one gridpoint point and level, only one of these fields can show a non-zero value. Although this is a direct diagnosis of wave breaking, its distribution as a global field at any one time is fragmented and does not readily show hazard areas. To produce a single variable, it was thus decided to look at several levels in a column, and flag the points where at any level between 450hPa and 150 hPa the value of the drag exceeded $10^{-5}ms^{-2}$. Hence a single field was derived in which each gridpoint was assigned a value of 1 where the drag exceeded $10^{-5}ms^{-2}$ in the column and 0 otherwise. For these purposes, this variable will be referred to in this section as the 'drag indicator'.

4.3 Aircraft data

The previous small-scale case study used a mixture of sources of turbulence encounter data, including both pilot (subjective) and automatic (objective) reporting systems. For this study, it was essential to use a consistent, objectively derived source of data, which includes null reports, as this is an essential requirement for development and verification of a prediction tool.

The archive of aircraft reports held by the aviation group accumulates several thousand such reports per day from aircraft equipped with ASDAR (Aircraft to Satellite DAta Relay) systems. These are made routinely during long-haul flights from a number of wide-bodied jets. Automatic sensors measure wind, temperature and vertical acceleration along with spatial and temporal information every 7 minutes during cruise phase of the flight. This data is stored along with corresponding model parameters for use in verification of forecasting techniques (see Rickard, 1997). Turbulence reports are derived from the vertical accelerations experienced by the aircraft relative to gravity, g. An index number between 0 and 3 is assigned, according to severity as shown in the table.

Turbulence reading	Acceleration as a factor of *g*
0	$g \pm < 0.15g$
1	$g \pm > 0.15g$
2	$g \pm > 0.30g$
3	$g \pm > 0.50g$

Table 4.2 Vertical accelerations related to turbulence index as stored in the CAT archive

Although a number of major long-haul routes are well represented, there are large areas for which this type of data cannot be obtained. This evidently limits the validity of the 'truth' dataset. However, it could be argued that the verification should concentrate on the areas with a high air traffic density, given that the customer for turbulence forecasts are air traffic operators for these routes. It should be noted though that the use of such localised data might influence the results as a global algorithm.

4.4 Data processing

The algorithm development was performed by matching representative UM data from a similar position and time to the actual aircraft reports available. Statistical tests on the relationship between the model fields described earlier and the positive and null turbulence reports from aircraft, formed the basis of testing the skill of the model fields in predicting turbulence events significant to aircraft. To obtain a scientifically useful subset of the vast numbers of reports available, various filter criteria had to be applied.

For each aircraft report used, model values from the derived stress and drag fields described above were extracted, taking the nearest gridpoint and level to the reported position of the observation. These were then treated as the dependent variables in the statistical process.

4.4.1 Filter criteria

ASDAR reports were extracted from the CAT archive for each day of the 21-day trial period. The model derived convective cloud top and base and the Dutton shear CAT probability associated with each report was also extracted for filtering the data.

Since the model runs were restricted to one per day, it was necessary to restrict the aircraft data used for the comparison to those within a few hours of the valid forecast time. The fields were taken to be representative of the situation several hours either side of the 0Z valid time, so only reports made between 18Z and 06Z for each trial day were included.

At this stage altitude restrictions were also imposed, since the algorithm is concerned with forecasting turbulence for upper air altitudes. The available model fields represented altitudes greater than FL230 (400hPa).

Having obtained the set of valid aircraft reports and associated model field values, these were filtered to eliminate those reports least likely to be caused by mountain wave activity, i.e. those in areas of predicted convection or shear-induced CAT. The final selection criteria were as follows:

- Reports from 18Z to 06Z for each 0Z run
- Reports over land areas only, reducing the data to 60% of the original volume to around 670 reports per day
- Reports whose position did not fall within the deepest model convection column (if any) of the four horizontally adjacent gridpoints

- Reports with Dutton CAT probability of 2.0 or less

After filtering the raw data, the dataset contained 5431 aircraft reports for the 21 day period, of which 131 (around 2.4%) of these were non-zero turbulence reports. All of these fell within the light turbulence (1) category.

4.4.2 Downstream turbulence considerations

The parameterised gravity wave fields in the model assume only vertical transmission of stress through the column from the surface gridpoints. There is no allowance for any horizontal transfer of the effects of wave activity onto adjacent points. However, there is evidence to suggest that turbulence from mountain waves at cruising levels can be felt some distance downwind from their source, as observed by Tilley *et al.* (1998). There is also reference to these effects in the forecasting guidelines of the Forecasters' Reference Book.

To include the effects of gravity wave activity upstream of a report position, field values from three gridpoints were considered as influencing the actual wave activity at the report position. Since mountain wave activity may often be felt up to 300km downstream of its source, it was decided to consider the model gravity wave parameters up to 2 gridpoints upwind of each reporting position. With the global model horizontal resolution at approximately 60-km in mid-latitudes, this would generally represent effects from points at least 120 km distant. In practice this distance may be greater since diagonally adjacent points are included and the grid-scale increases for lower latitudes.

Wind fields were available for three standard levels: 300, 250 and 200 hPa, for use in determining the wind direction and hence upwind points. Both the gravity wave stress and drag as well as the wind fields are all output on the U-grid of the model, eliminating the need for interpolation of any field onto a staggered grid. Since the wind field heights are defined in terms of pressure, they could easily be compared with the pressure of each reporting location to determine which wind field to use for each data point.

For the purposes of this study, the maximum value of either stress or the drag indicator over the three points was taken as the independent regression variable.

4.5 Coding details for selection of model points

The three gridpoints related to each aircraft report position were defined according to the following process:

Vertical mapping: The model level from which to take the gridpoint values was calculated using the corresponding surface pressure field for the same model run and forecast time, and calculating the pressure heights of the levels at each gridpoint using the appropriate A_k and B_k values. These are distinct for stress and drag fields, since stress is output on half levels and drag on full levels. For each aircraft report, the model level with the nearest pressure to that of the report was used.

From the available wind fields (200, 250 or 300 hPa), the nearest pressure level to the reported pressure at the aircraft position was used to determine a representative wind direction.

Horizontal mapping: The U and V components of each of the three fields were combined to produce a magnitude field for the stress and two drag fields. Values were taken from the nearest model grid point on the staggered (U-grid) of the UM. This was used as the first representative point for each report position. Interpolation from other

surrounding points was not performed partly because this can smooth the stress fields too much and partly because a final operational product would also not be smoothed.

From the wind direction calculated from the appropriate level, the adjacent upwind gridpoint was determined as shown in figure 4.1. The threshold angles were chosen such that there was equal weighting given to diagonally adjacent gridpoints as well as directly adjacent points. In figure 4.1, the areas enclosed between each pair of diagonal lines are equal within the outer square of 8 gridpoints.

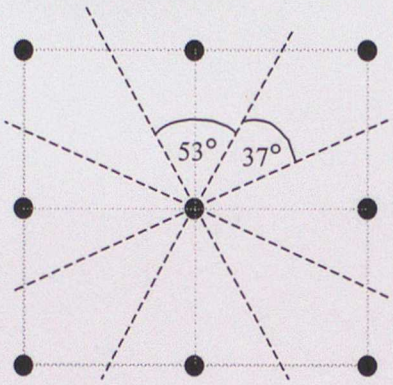

Figure 4.1 *Selection of upwind points relative to wind direction*

Similarly, the second upwind gridpoint was determined using the wind direction vector at the first upwind point, thus using the most local wind information to determine the second point. This is illustrated below.

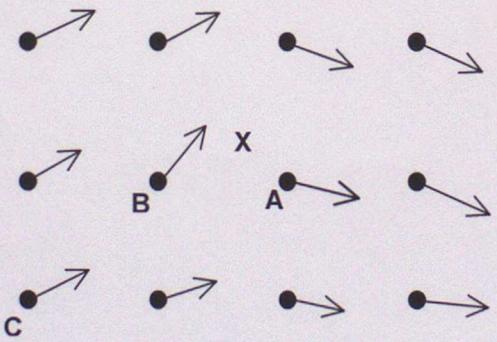

Figure 4.2*: Illustration of how upwind points were selected for analysis. Point X represents the report position, A the nearest point (regardless of wind direction), and B and C the first and second upwind points respectively. Thus the effects experienced at X are considered to be related to the gravity wave parameters at these three points*

It should be noted that wind direction was not considered in the determination of the nearest point, regardless of whether this was upwind or the report position or not. In an operational prediction scheme, it is effectively the diagnostic at the nearest gridpoint, which will define whether a turbulence hazard is present.

4.6 *Statistical analyses and results*

Using the aircraft turbulence indicator as the dependent variable and combinations of stress magnitudes and drag indicators as independent variables, regression analyses were performed. The aim was to find a predictor which gives the optimum combination of the 'hit rate' (the most positive events associated with model predicted 'hazard' points) and 'false alarm rate' (the number of null reports which are predicted as 'hazard' points).

From consideration of the theory and case studies, data points with associated high stress model values were expected to show a higher frequency of positive (index value 1 or greater) turbulence reports than those with low stress model values. Areas of particular risk are also likely to be associated with wave breaking and hence have a non-zero drag (deceleration) value. This should indicate the locations of predicted turbulence and hence a hazard area. From these analyses threshold values in a predictor field should then be associated with a consistent probability of a turbulence encounter, which then forms the quantifiable forecast for MWT.

Separate scores were produced, firstly considering only the nearest gridpoint values and secondly including the maximum value of the two upwind gridpoints, in order to assess the added value (if any) of representing downstream effects in a prediction scheme. To maintain simplicity, no actual distinction was made between the first and second upwind points at this stage.

Since mountain wave effects generally occupy much of the vertical column, the vertical resolution of the model is less critical in detecting the hazard areas than it is for shear-induced CAT. The horizontal resolution is more critical, as it affects the wavelengths of gravity waves that are resolved and the accuracy of the orographic variance, which is highly influential on the parameterisation results. Taking these considerations into account, a predictor which displays similar or better skill than those existing for shear-induced CAT (see Bysouth, 1998) is expected.

4.6.1 Means Comparison

Having crudely filtered the raw aircraft reports to eliminate other likely causes of turbulence, it is expected that there should be a significant difference in the associated stress values between turbulence reports and null reports. The first test was to determine the mean and standard deviation of the stress magnitudes at the nearest points.

	Turbulence Index	N	Mean	Std. Deviation	Std. Error Mean
Stress (nearest)	1	131	2.452E-02	6.414E-02	5.604E-03
	0	5300	1.157E-02	3.441E-02	4.727E-04
Stress (maximum)	1	131	4.289E-02	0.114	9.983E-03
	0	5300	1.754E-02	4.748E-02	6.522E-04

Table 4.3: *Table showing means and standard deviations of the stress values associated with turbulent and null reports, using the nearest point only and then the maximum of the two upwind points. Note that the means are greater for turbulent reports*

The mean stress value at the nearest gridpoint for turbulent points was higher by a factor of around 2 than for null points. However, the strong bias towards zero values also results in the doubling of the standard deviation. This effect is even more apparent when considering the maximum stress value of the upwind gridpoints. Here the turbulent points had a mean stress 2.44 times greater than the non-turbulent points, again with a corresponding increase in standard deviation.

A t-test was performed to compare the mean stress values between turbulent and null reports. It was found that with 97% confidence, turbulent reports had a greater associated mean stress value (both locally and upwind) than null reports. Hence it may be concluded that the gravity wave stress field can demonstrate some skill in predicting areas of MWT.

	t-test for Equality of Means						
	t	df	Sig. (2-tailed)	Mean Difference	Std. Error Difference	97% Confidence Interval of the Mean	
						Lower	Upper
Stress (nearest)	2.304	131.856	.023	1.296E-02	5.624E-03	6.1933E-04	2.5296E-02
Stress (maximum)	2.533	131.112	.012	2.534E-02	1.000E-02	3.3938E-03	4.7291E-02

Table 4.4: *Results of a means comparison between stress value means for turbulent and null reports. In both the cases shown, the range of differences between the means (shaded cells) at the 97% confidence level do not include 0. Hence, the two sets of reports have significantly different mean stress values at this confidence level. Equal variances were not assumed in this analysis*

As described earlier in this chapter, the acceleration fields were modified such that a grid point was flagged as positive if the maximum value of the drag within the column of 14 levels exceeded a value of 10^{-5} ms^{-2}. As such, performing a t-test on discrete logical values was not possible.

Out of the 5431 filtered aircraft reports, 902 (16.6%) had an associated nearest point drag indicator of 1, i.e. stress deposition (drag) was diagnosed at those points. For the positive turbulence reports only, this proportion increased to 22.1%. Corresponding scores of 25.2% and 28.2% were shown when upwind points were included.

This simple analysis showed that in areas where wave breaking is diagnosed, there is an increased chance of an aircraft encountering turbulence than in areas of low stress and where no wave breaking is diagnosed.

4.6.2 Regression analyses

Linear regressions were performed using combinations of the two variables, again using nearest gridpoint and upwind values in turn. Since the dependent variable (aircraft turbulence indicators) contained only values of 1 and 0, a logistic regression was performed against the continuous stress magnitude values. This process attempts to fit a linear solution to the scatter of 1s and 0s.

The predicted quantity, denoted as TE, may be considered as a turbulence estimate. Although this value is not directly meaningful, it can be used to define thresholds corresponding to actual stress values which may be used to define thresholds by which skill scores can be calculated and in turn a turbulence encounter risk may be quantified.

The regressions showed a weak positive dependence of the reported turbulence index on the stress value ($R^2 < 0.1$). This weakness was largely due to the large number of null reports. The linear regression equations for various combinations of the model variables are given in table 4.5. A typical linear plot is shown in figure 4.3. The maximum value lies at around 0.3, which correspond to maximum stress magnitudes of the order of 2 Pa. In order to calculate skill scores, certain TE values were used as test thresholds to delineate CAT and non-CAT events. The 75^{th} percentile threshold of TE was defined as the value where 25% of aircraft reports had TE greater than that value (figure 4.3). The 85^{th} and 95^{th} percentile TE values were similarly defined for each regression and shown in table 4.5. These percentiles were chosen to match the estimated proportion of positive reports to null reports i.e. 5 – 25%. Where only one variable was used, a TE value can be translated directly to a threshold stress value.

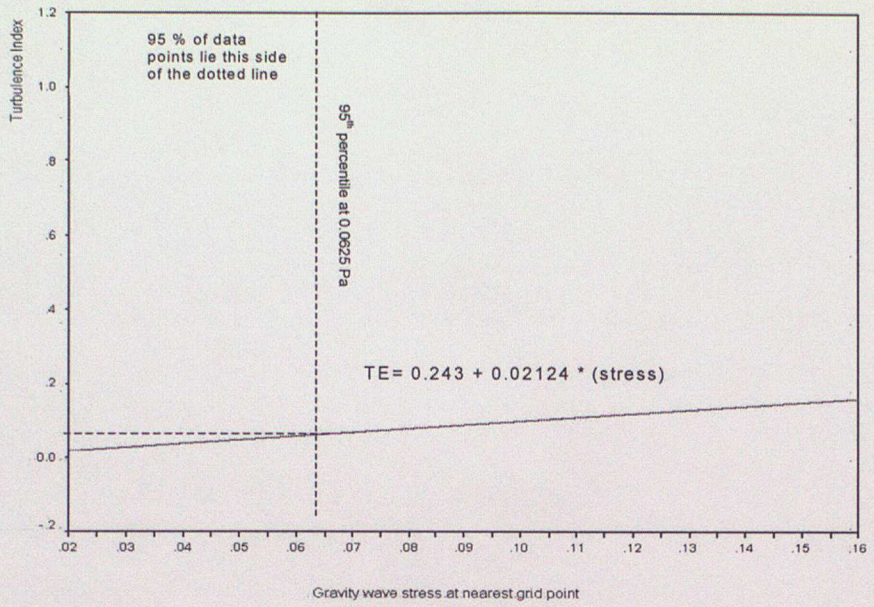

Figure 4.3: *Logistic regression showing derived turbulence indicator equation, and the position of the 95th percentile value for stress magnitude. This means that 5% of the points have stress magnitude values greater than 0.0625.*

Variables used in regression	Predictor equation (TE=turbulence estimate)	75% Threshold	85% Threshold	95% Threshold
Stress (nearest)	TE = 0.0212 + 0.243 * stress	.02291	.02522	.03639
Stress (maximum)	TE = .01984 + 0.236 * stress	.02303	.026	.04207
Stress (nearest) Drag (nearest)	TE = 0.02086 + 0.233*stress + 0.002979*drag_indicator	.02383	.02622	.03697
Stress (maximum) Drag (nearest)	TE = 0.01968 +0.234*Stress + 0.001193*drag_indicator	.02310	.02620	.04227

Table 4.5: *Linear regression equations for different combinations of model variables. Threshold values of TE for 75th, 85th and 95th percentiles relating to these equations are also given (see text for explanation)*

The regressions were performed with combinations of stress and drag indicators, for both nearest point values, and maximum of the upwind points. However, when including upwind values for the 'drag indicator', negative coefficients resulted, so the variables were discarded, since they could not be considered independent.

4.6.3 Skill scores

For each percentile threshold and regression equation, aircraft reports for which TE values were greater than this cut-off TE value were treated as positive (yes) predictions for MWT hazard, while those lower than the cut-off were treated as negative (no) predictions. The aim was to find the best regression equation and threshold to maximise the coincidence of actual turbulence reports with the 'predicted' turbulence points (i.e. an optimum hit rate), whilst minimising false alarms. This would then form the basis for an operational algorithm.

Contingency tables were constructed for each of the three defined thresholds in turn and for each regression equation. Various scores can be derived from these: -

	Reported 0	Reported 1
Predicted 0	A	B
Predicted 1	D	C

- Total null ('no') reports: A+D 5300 from filtered data
- Total turbulence ('yes') reports: B+C 131 from filtered data
- Total reports: A+B+C+D 5431 from filtered data
- Hit rate (HR)/Probability of detection (PoD): C/(B+C)
- False alarm rate (FAR): D/(C+D)
- Probability of CAT in predicted 'yes' area: C/(C+D) 1-FAR

Hit rates and false alarm rates were calculated in each case. In addition to the three percentile threshold values, a stress magnitude threshold of 0.01 Pa was also tested, as a reference first guess value, found in the Alps case study (Turner, 1997).

The stress thresholds corresponding to the TE values and skill scores for each of the regressions are shown in table 4.6.

a)

Predictor	Threshold percentile (from regression)	Threshold stress magnitude (Pa)	Hit rate	False alarm rate
Nearest point	75	0.007	36.6	96.5
	80	0.01	33.6	96.0
	85	.0165	31.3	95.0
	95	0.0625	9.2	95.6
Max of 3 upwind points	71	0.01	39.7	96.7
	75	0.0135	38.9	96.2
	85	0.020	31.3	95.0
	95	0.086	10.7	94.9
Drag at nearest point	N/A	N/A	22.1	96.8
Max drag from 3 points	N/A	N/A	28.2	97.3

b)

Regression variables	Threshold percentile	Hit rate	False alarm rate
Nearest stress + drag indicator (nearest point)	75	39.7	96.3
	85	29.0	95.4
	95	8.4	96.0
Max stress (3 points) + drag indicator (nearest point)	75	38.2	96.3
	85	32.0	94.9
	95	10.7	94.9

Table 4.6 a) *Stress magnitude cut-off values and their hit rates and false alarm rates for signal variable regressions* ***b)*** *Hit rates and false alarm rates for multiple variable regressions*

4.7 Discussion of results

The skill in a regression experiment can be judged by two scores. The hit rate (HR), should be as high as possible, indicating a high percentage of the actual encounters are predicted. Conversely, the false alarm rate (FAR), should be minimised, preventing excessively large predicted hazard areas with low probability of an actual event occurring.

The dominance of zero reports which are present even in 'turbulent' areas provide a hindrance when using these statistical methods, since any result will incur a very high false alarm rate. The fact that this verification data originates from actual flights means that wherever pilots can avoid known areas of turbulence they will do so. The dataset is biased towards minimal turbulent activity. These points should be borne in mind when considering this work.

Stress values only

Considering the nearest point stress value only, the hit rates were around 36% at best. This indicates that over a third of all the turbulent reports, which may be due to mountain, waves are being detected. When the maximum value of all 3 points is taken, the hit rate rises to 39% at the 75^{th} percentile threshold. However, since the stress cut-off value is low, the false alarm rate is increased, and large areas of low risk would be defined as hazard regions.

When considering upwind stress values, the hit rates increase, by around 4% for the 75% threshold, and by around 1% for the 95% threshold. The false alarm rates also to decreased slightly, with the optimum combination at the 85% threshold, with HR of 31. %, and FAR of 95%, only 0.1% higher than the minimum. The cut-off stress value in this case is around 0.02 Pa. This shows that the influence of upwind wave activity is significant and should be accounted for in the predictor.

Wave breaking diagnostics

Since the drag indicator was a discrete 0 or 1 field, the contingency table could be directly derived without regression. The hit rates were lower than for the stress fields, but had the highest false alarm rates. The inclusion of upwind drag points improved the hit rates by 6%, further supporting the significance of downstream effects.

Stress and drag fields

When combining upwind drag points with the stress fields, negative coefficients resulted, indicating non-independent variables and were discarded. Hence, the nearest point drag indicator was combined with both the nearest point stress values, and the upwind maximum.

The scores show similar skill to the stress only regression, but with improved FAR. However, when considering that the drag indicator is a much simplified derivation of the original fields, and any algorithm using it would require these fields to be made available, the improvement in skill does not seem sufficient to justify its use.

4.8 Conclusion

The statistical tests presented in this section have shown some skill in predicting MWT events using the gravity wave drag fields from the global model. The influence of the drag fields on this skill is less apparent than that of the stress magnitude.

The hit rates are far more sensitive than the false alarm rates to the choice of threshold value. At best only around one third of the possible MWT events have been correlated with stress activity. An examination of the missed points may reveal possible reasons for this (e.g. cloud cover, stronger downwind effects than allowed for). Overall, the scores are better than those for the shear-induced CAT predictors, where the hit rates are typically less than 10%.

The inclusion of upwind points in the predictor leads to slight improvements in both the hit rate and false alarm rate. It should also be noted that the threshold values using the same percentiles are slightly higher. The hit rates and false alarm rates in the final regression involving the upwind points are at least as good as those using just the nearest points to the observations.

The overwhelming dominance of null reports, even within areas of active turbulence distorted the results from regression tests. In finding an effective algorithm, the hit rate must be optimised without significant detriment to the false alarm rate. Care must be taken however, not to lose the skill in predicting hazard areas by always forecasting the same mountainous regions, regardless of the meteorology.

When comparing these scores with other schemes in an operational environment, it must be remembered that these experiments were performed using T+12 fields, rather than the T+24, which are required for operational WAFC forecasts. Thus, the scores here are better than would be expected for an operational algorithm.

Since the stress and drag fields were not originally available from the daily forecast model runs, there must be sufficient justification in using them in a predictor to offset the computational time and storage costs involved. It is clear that the gravity wave stress fields show the most skill, while it appears that the addition of drag fields does not improve the scores significantly enough to justify extra computational overheads.

The results of this study were further used in a real-time developmental project to test a trial prediction scheme intended to assess the usefulness and usability of a mountain wave algorithm in SIGWX chart production. This will be described in the next chapter.

5 Real time winter trial

5.1 Introduction

The statistical analyses presented in the previous chapter showed that global gravity wave stress fields from the UM showed skill in prediction of MWT events comparable with that shown by existing shear CAT predictors. It was also found that when taking the wind field into account, this skill improved, due to the representation of downstream effects of gravity waves. This suggests that the use of a MWT 'first guess' predictor using these results could significantly enhance the CAT forecasts made as part of the WAFC responsibility.

Before such a scheme could be implemented as an operational forecasting tool, it first had to be tested and monitored in the context of its intended use. The purpose of this was to define the details for the presentation of the final predictor field and highlight any improvements, which could be made which were not evident in the development stage. Finally, it was necessary to quantify its usefulness when considered as part of the whole range of forecasting tools available to the forecaster. This chapter describes the winter trial, which was conducted to address this need.

Throughout the trial, modified gravity wave stress fields from daily model runs were made available to duty WAFC forecasters. It was intended that the forecasters would comment on whether they could use such an additional field to enhance their current CAT forecasts and whether the presentation format was useful or could be improved. This trial covered a 5-week period in late 1998. Both forecaster feedback and objective verification results were used to provide a case for whether or not a MWT predictor should be implemented for operational use.

5.2 Aims of the trial

- To further verify the chosen algorithm in a real time sense during a northern hemisphere winter period (the most active period for mountain waves)
- To assess the variability of the defined 'hazard areas' in varying meteorological conditions for key areas of the globe
- To determine the best use of the available fields to provide a first guess for MWT risk areas
- To determine threshold stress values which provide most value in a first guess field
- To establish how the field(s) should be presented on-screen for clarity and ease of use
- To gain the opinions and comments of the WAFC forecasters
- To quantify the strengths and limitations of the suggested scheme, and determine areas for future refinement
- To gain enough information to be able to recommend implementation of a MWT predictor

5.3 Algorithms and parameters used

In the previous section it was established that although gravity wave drag fields added some additional skill in capturing turbulence events, this was not significant compared to gravity wave stress fields alone. Therefore in this trial, the experimental chart products were based purely on the stress fields available from the two main global model runs, with data times 0Z and 12Z. From the single variable regressions, the prediction parameter (TE) for MWT activity was linearly related to a stress magnitude value. Thus the cut-off thresholds identified were directly translated to threshold stress values.

The principle problem for the trial product was that of representing heights of high stress areas. When associating stress values with actual aircraft reporting points, values from the nearest vertical level were taken, so as to be as representative as possible of the reporting position. However, since there are around 14 model levels, which cover the altitude range required for SIGWX charts, it is clearly impractical to produce separate forecasts for each level. Therefore some kind of approximate representation had to be made.

The altitude range was represented the in 2 layers, one covering FL250 - FL350 and the other from FL350 - FL450. Selecting the levels relating to these was non-trivial, since the actual heights they represent vary with the underlying orography, as represented by the model surface pressure field[1]. The lowest model surface pressure for all but the highest points in the Himalayas was around 500 hPa. Estimates of the pressure heights of model levels using 1000hPa and 500hPa as extremes in surface pressure identified which levels were appropriate for the height range required (table 4.1). A conversion table was used to translate these into flight levels.

Model level	Pressure at model level		Equivalent flight level	
	P* = 1000hPa Sea level	P* = 500hPa Mountain	P* = 1000hPa Sea level	P* = 500hPa Mountain
12	500	301	180	300
15	370	255	250	340
19	265	207	330	380
23	165	146	420	450

Table 4.1 *Equivalent flight levels for selected model levels over low and high ground. The requirement was for a model level range covering FL250-450, especially over high orography. Levels 12-23 were selected*

Levels 12-23 inclusive were used to generate two stress fields, representing the lower and upper 'halves' of the atmosphere in the range of interest: levels 12-17 for FL250-350 and 18-23 for FL350 and above. This gave 6 levels for each 'half'. At each gridpoint, a maximum value was taken from the 6 levels in the column, to generate a 'worst case' predictor field for half of the altitude range. This approximation was expected to slightly increase hit rates in the verification, since maximum values were used in the column, rather than the nearest individual gridpoint.

5.3.1 Downwind effect

The charts produced did not show fields, which included the downwind effect. However, it was pointed out to the forecasters that the areas marked may extend further in the direction of a strong upper level flow and this was taken into consideration. However, for the objective verification using the ASDAR turbulence report archive, scores for both the unmodified stress field and with downwind effect represented were calculated and compared.

---

[1] Model (Eta) level pressure, P at a gridpoint is given by $P = A_k * PREF + PSTAR * B_k$, where $PREF = 10^5$ Pa (Reference sea level pressure), and $PSTAR$ is the model surface pressure (variable with orography)

5.4 Chart Products

The two resulting stress fields were plotted onto appropriate chart areas, with coloured contours added to delineate different hit rates. The associated hit rates were provided for information. This formed the 'first guess' sample product.

WAFC charts are produced four times daily and are constrained to use forecast fields from the 0Z and 12Z runs of the global model. During this trial, a set of charts relating to a single forecast time only each day was provided to the WAFC bench.

It was found to be most practical for T+24 fields from the 0Z global model run to be used in the trial. The relevant charts could be produced early in the morning and taken down to the NMC at around 9.30am, when the forecasters were beginning production of the set of WAFC charts valid for 0Z the following night.

The two height fields of stress magnitudes as described above were produced for five different chart areas. The coverage of these differed from the standard six chart areas, in order to best show the continental landmasses. Two charts were plotted on each page, with the maximum stress magnitude for FL250-350 plotted above that for FL350-450, for each continental region.

5.4.1 Contour values used

Initially, 2 contour values were chosen to be represented, relating directly to the threshold predictor variable derived in the previous chapter, and with their associated skill scores:

- 0.007 Pa 3.5% Probability of encountering turbulence
- 0.0625 Pa 4.5% Probability of encountering turbulence

The low stress contour was marked in blue, and the high stress contour in red. These were chosen to show broad areas of gravity wave activity (the .007 contour) while highlighting those points with particularly high stress values (.0625 contour) and hence a higher risk. Since one of the purposes of the trial was to establish the best contour values to use, modification of these was expected during the trial progress.

The chart areas produced, with the contours marked are shown in figure 5.1.

5.5 Role of WAFC forecasters in the trial

The principle purpose of producing charts regularly over a period of a number of weeks was to gain feedback and suggestions from the final users, the forecasters, on the product and its usefulness in an operational context. Producing fields over a continuous time also gave the opportunity to assess the variability in the diagnosed MWT risk areas from day to day and with changing synoptic situations. This was important to avoid producing a field, which consistently highlights the same orographic areas, with little dependence on meteorology.

In many cases, the areas highlighted by the fields coincided with those already indicated as hazardous due to shear-induced CAT. It is reasonable to assume that the presence of an upper level jet oriented perpendicularly to a mountain range may also enhance the gravity wave stress in the UM, and so turbulence can result from a combination of the two phenomena. However, the purpose of developing a separate MWT predictor is to identify regions susceptible to MWT in the absence of other sources of CAT. The trial aimed to highlight the extent to which this was the case and how useful it was as an indicator of actual turbulence.

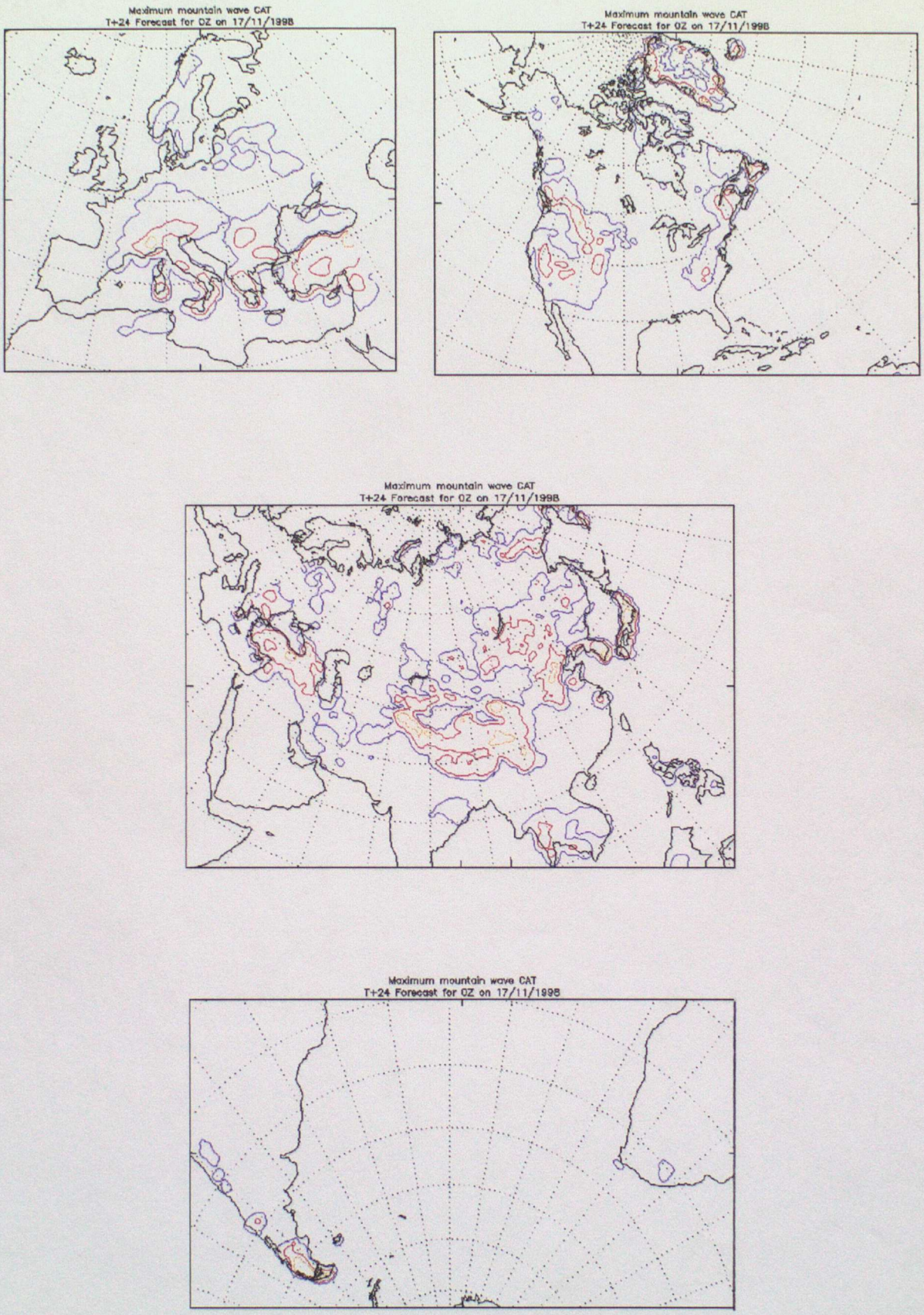

Figure 5.1 *the five chart areas used in the trial. Here, contours at three values are shown: 0.007 Pa (blue), 0.0625 Pa (red), and 0.25 Pa (orange). Africa and the northern part of South America are omitted as turbulence events in these regions are dominated by convective activity, with little mountain wave effect.*

Forecasters were asked to comment on these points, as well as give their general impression of the charts, including the contours used, the height representation and the overall presentation. In general, the forecasters indicated areas of concern or interest on the paper charts provided, made notes of general comments. Direct contact was made daily after the forecast had been completed and dispatched and copies of the final SIGWX charts taken for comparison with the stress products.

A web page was created on which the progress reports and feedback were posted at regular intervals during the trial. This was available to everyone involved, particularly to enable shift-working forecasters to easily keep up with trial progress. Various changes were made during the period in direct response to their input. These will be described later in this chapter.

5.6 Objective Verification

For the days on which charts were provided to the forecasters, ASDAR aircraft reports from the CAT archive were extracted for reports made within 3 hours of the forecast valid time (i.e. from 21Z the previous day to 03Z the same day for 0Z valid time). The convective cloud amounts for the surrounding gridpoints were used to eliminate those reports, which were most likely to have occurred around convection.

The maximum stress magnitude for the appropriate one of the two height ranges was extracted from the nearest gridpoint to each of the report locations. This value was then used to construct contingency tables and skill scores calculated relating to each of the three identified threshold values, following the procedures described in the previous chapter.

The skill scores were expected to differ slightly from those generated from the regression in the previous chapter. Firstly, the regression analysis used T+12 fields as the prediction variable, while the operational requirement is for T+24, which was used here. Hence the additional spread in stress values from the 'truth' would cause a slight detrimental effect on the skill observed. Conversely, the use of the maximum stress value in the column, as opposed to the nearest model level, has the effect of the stress values associated with the report being slightly higher, which should increase the hit rates. The net result of these will influence the final scores.

Although the downwind effect was not plotted on the charts given to the forecasters, the verification was performed, not only on the stress fields alone, but including the downwind effect also. It was expected that the inclusion of this effect would increase the skill of the predictor.

5.7 Results

5.7.1 General comments and trial progress

Throughout the period of the trial, comments were made by the forecasters of their impressions of the charts produced and the usefulness of the field as a tool in SIGWX forecasting. A number of amendments were made in response to these comments and are summarised along with the dates, general meteorological descriptions and objective data availability in figure 5.2. The dates correspond to the 0Z-validity time.

Month	Day	ASDAR data analysed	Chart details, changes made, comments
Oct	23		18Z fields, standard chart areas, contours at .007 and .0625 Pa
	26		Large areas marked seem to outline main mountain ranges. Strong signal over central Europe / Turkey
	27		0Z fields, standard chart areas, still strong over Europe/UK/Turkey - shear CAT over Alps forecast
	28		Strong signal over UK, surface chart analysed and showed strong low level westerlies
	29		
	30		Continued large area of >0.0625 Pa activity across Europe - unusual?
	31		Contoured areas judged too extensive over Asia for a useful forecast Downstream effects queried Rocky mountains showed high activity initially, and then dropped dramatically Africa showed little or no hazard areas Australia/NZ variable with wind direction. Southern Alps commonly highlighted as hazard area
Nov	3		Significant signal seen over Eastern Greenland, previously not present. Forecasters found this area useful
	4		
	5		Central Europe/Spain still showing high activity, reducing by end of week.
	6	✓	
	7	✓	Areas over central Asia much reduced, but still too extensive for CAT areas to be marked on SIGWX chart ASDAR data available from 6 November for objective verification
	10	✓	New chart areas (continental land masses) plotted
	11	✓	.007 contour omitted, .25 Pa contour added
	12	✓	Europe/UK region less active and much more variable
	13	✓	Rockies more variable, new contour good for highlighting particularly hazardous areas)
	14	✓	Consistent high stress over extreme south of S. America
	17	✓	Mountain wave CAT area (central Rockies) forecast on SIGWX chart 11 AIREPs reported turbulence (2 moderate) occurred within predicted region. No ASDAR reports available from that region
	18	✓	Much reduced activity over Greenland
	19	✓	Forecasters gain confidence with the product, and begin to mark highlighted areas in addition to shear CAT areas.
	20	✓	
	21	✓	New contours show more useful areas.
	24	✓	Additional CAT areas marked on SIGWX chart due to mountain wave activity over Rockies, S. America and Himalayas.
	25	✓	
	26	✓	Break for data processing / verification / review of progress
Dec	15	✓	Active areas over the N. Rockies, the Alps and over UK. Presence of jets probably enhanced the signal
	16	✓	
	22		At request of WAFC forecaster
	23		At request of WAFC forecaster

Table 5.2 *General comments and summary of trial progress and verification data used*

It was consistently found that little or no MWT areas occurred over the whole of Africa. It appeared that the only areas susceptible were the Atlas Mountains and the southern tip of South Africa, both of which could be included in charts of the other continental regions. It was decided then to not produce a chart of Africa alone. Similarly, the main part of South America was not plotted, as turbulence encounters in this region were almost always convective in origin. The southern tip of South America was included in one of the other chart areas (see figure 5.1).

At the end of week 1, it was clear that the blue contours outlined very large areas of high ground and although they did vary with the meteorological situation, they were considered too extensive to be of much use. The red contours showed more useable region sizes, but forecasters requested more detail within these areas. In response to this, the blue contour was dropped and a new one, at 0.25 Pa was introduced. Objective verification was performed on all three-threshold values.

The two height ranges displayed very similar fields in most cases, indicating that the maximum stress is about equal for the two 'halves' of the altitude range considered. The forecasters were concerned about this and requested some kind of height indicator field to show the extent of the high stress regions. The main area of concern was how the position of the tropopause affected the stress deposition.

In general, by the 5th week of the trial, the regular forecasters were familiar with the charts and the areas where there was most variability and potential to add value to the CAT forecasts. On a number of occasions, the CAT areas were modified to incorporate mountain wave activity highlighted by the contour plots. This was an encouraging end to the trial.

5.7.2 Objective verification results

Skill scores were calculated using the techniques described in chapter 4, for each of the stress values used as contours on the trial charts. The aircraft report data quantity was as follows: -

- Number of days verified 17
- Total number of aircraft reports 6649
- Number of turbulence events (1 or greater) 330 (5%)

The scores were calculated using totals from the whole 17-day dataset. The results are shown in table 5.3. The peak single day hit rate is also presented, as an indication of the maximum skill achieved. The first row shows the scores when only non-shear CAT reports are considered (i.e. those with a Dutton index of 2.0 or greater eliminated). The second and third rows show scores on the whole set of reports for the unmodified and downwind modified stress fields respectively. For simplicity, the reports were verified against the maximum stress field for the whole height range, rather than for each half as presented in the charts.

An ideal predictor should display a high hit rate (HR), capturing most of the actual turbulence events within the predicted area. This can be automatically achieved by specifying large hazard areas, with very little skill. To safeguard against this, a predictor should also minimise areas of over-forecasting and hence have a low false alarm rate (FAR). The 'probability of encounter' (1-FAR) gives a direct indication of the risk associated with each threshold stress value. An optimum high HR and low FAR is required for a skilful prediction system.

The scores presented here seem to show less skill in predicting MWT than that found in the previous study. However, it must be remembered that increased error is expected in the use of the T+24 fields used here, compared with the smaller lead-time in the development study. Through the 17 days for which data was available, considerable variability was seen between the number of daily turbulence events, causing the scores to fluctuate over the trial period. An analysis of the peak single day values shows more comparable results.

The low hit rates shown in these results indicate that many of the positive turbulence reports occurred outside of the contoured areas. This may be due to model errors in the positions of hazard areas and some genuine MWT turbulence events may have been reported from positions close to contoured areas. Alternatively, these 'missed' events are likely to be due to other sources of turbulence, either shear-induced CAT or convection. Although the UM can indicate areas of convection and uses the Dutton index for shear-

induced CAT prediction, neither scheme can be assumed to capture all events which are caused by these phenomena.

The elimination of diagnosed shear-CAT reports did not show any improvement in the skill of the stress field predictor. This supports the reasoning that mountain wave events commonly coincide with conditions, which lead to shear-induced CAT and indeed may contribute to the conditions required to produce CAT. Although the development of the predictor is to address areas where other sources of CAT are not present, the elimination of these effects gives a false picture of the effects it aims to diagnose. The hit rates and probabilities of encounter both improved when considering all the reports, which may or may not have shear-induced CAT contributing to the effects.

The false alarm rates for the highest stress threshold, 0.25 Pa, are significantly lower than for the other thresholds, indicating that the risk of encountering turbulence is increased within these high stress areas. This shows that there is a strong connection between high gravity wave stress areas and hazardous turbulence events. The use of this contour in a final forecast product will therefore be useful in pinpointing the most susceptible areas to MWT, and the associated increased severity of an encounter.

It should be remembered that the data used in this verification study is constrained to the regular flight paths of long haul flights. Inevitably there are many regions of the globe, which were not verified as part of this study.

a) 0.007 Pa threshold

	Hit Rate		False alarm rate	Encounter probability
	Total	Peak		
Maximum stress, levels 12-23, shear CAT eliminated (Dutton CAT prob > 2.0)	11.0	33.3	95.8	4.2
Max stress, levels 12-23, shear CAT not eliminated	14.2	36.0	95.6	4.4
Max stress, levels 12-23, shear CAT not eliminated, downwind stretching included	13.9	33.0	96.0	4.0

b) 0.0625 Pa threshold

	Hit Rate		False alarm rate	Encounter probability
	Total	Peak		
Maximum stress, levels 12-23, Dutton shear CAT eliminated	3.1	18.8	95.7	4.3
Max stress, levels 12-23, shear CAT not eliminated	3.6	20.0	96.0	4.0
Max stress, levels 12-23, shear CAT not eliminated, downwind stretching included	4.5	25.0	96.1	3.9

c) 0.25 Pa threshold

	Hit Rate		False alarm rate	Encounter probability
	Total	Peak		
Maximum stress, levels 12-23, Dutton shear CAT eliminated	0.9	6.3	88.0	12.0
Max stress, levels 12-23, shear CAT not eliminated	1.2	12.5	87.5	12.5
Max stress, levels 12-23, shear CAT not eliminated, downwind stretching included	1.5	6.3	89.8	10.2

Table 5.3 *Hit rates and false alarm rates (shown as percentages) for each of the three threshold stress magnitude values considered. The encounter probability (1-FAR) is also given as a direct measure of turbulence risk. These scores were calculated using the unfiltered data set, since shear CAT events may also be MWT events*

5.8 Pre-Implementation survey

After completion of the trial and the verification, the results showed that there was considerable skill to be gained from the use of gravity wave stress fields in prediction of MWT. However, if the scheme were to be introduced operationally, its success ultimately depends on the support of the forecasters, whether the product is usable and practical for enhancing the CAT products in the short timeframe they have to produce WAFC charts. Hence, to make a final case for implementation, forecasters were consulted for their opinions on the operational use of the MWT predictor as used in the trial.

A short summary of the results of the trial and the proposed final presentation of the single-field product was published on the Intranet and 14 regular WAFC forecasters were invited to respond to 4 questions, by e-mail. 8 Replies were received.

The questions and responses may be summarised as follows: -

1. **Would this indicator of mountain wave turbulence be useful and worthwhile to WAFC forecasters?**

   All the responses were positive to this one. The general opinion was that it would be a useful addition to the existing CAT field, although it is recognised that much of the areas it highlights would already be covered by the shear CAT.

2. **Is a single field with the two suggested contour values (.0625 and .25 Pa) sufficient for its effective use?**

   Most respondents agreed to the single field, although there was concern that there is no height indication of the most hazardous areas. Experience during the trial showed this to be around FL350 +/- 5000 ft. However, a second field would be required to display associated height, hence incurring more computing and storage overheads. It could be argued that specifying the altitude for MWT is less important because, unlike the shear CAT, the effects are generally felt over a large altitude range, making it difficult for a flight path to avoid a hazard region by changing altitude.

   The contour values at .0625 Pa and .25 Pa were generally accepted as useful for highlighting hazard areas, and showing particularly strong signals, while avoiding excessive coverage. The contour at .007 Pa was judged too extensive.

3. **Would you be willing to use this extra field to enhance current CAT forecasts on WAFC charts?**

   All respondents said they would be willing to use the field, although perhaps a little cautiously at first. To aid the introduction of the scheme, documentation explaining the derivation and use of the field would be made available to the forecasters.

   Once implemented, the performance of the predictor would be continuously objectively verified by the Aviation research group, and feedback from the bench would also be welcomed.

4. **If you have concerns about the implementation, please summarise them briefly.**

   Confusion with shear CAT:
   Forecasters stressed the need to keep the new field separate from the existing shear CAT predictor. The MWT predictor has been developed as a separate tool, intended to be used in support of the existing fields and will be a separate field in its own right. The final decision as to whether or how much to use it lies with the forecaster.

Severity vs. probability:
As with the shear CAT verification, the skill scores are based on the turbulence reports from ASDAR, which are almost all reports of light turbulence (but from the biggest aircraft, so could be equivalent to moderate/severe for smaller aircraft). The probabilities are also based on these data.

From looking at other sources of turbulence data (AIREPS, pilot reports), there is evidence to suggest that areas of high risk according to the predictor, are also associated with moderate or severe turbulence events, and should be treated as such for the purposes of the WAFC requirement. Experience should clarify this.

Height indication
As discussed above, there was concern about how to forecast the height extent of the risk areas. It is anticipated that with experience of using the field and knowledge of tropospheric heights will adequately compensate for a more objective height field, as the vertical variation in the fields is not as sensitive as that for shear CAT forecasting. Future capacity to display further fields may justify a height estimate.

5.9 Summary of trial project outcomes

The execution of the winter trial project was intended to identify and address issues and potential problems between the stages of algorithm development and implementation into the operational environment. Overall the trial was extremely successful and the aims were largely met and problems overcome.

The prediction scheme developed from the regressions described in chapter 4 was further verified using objective reports, using T+24 model field data, as would be used in WAFC forecast products. Results showed comparable results, allowing for the expected increased error and the restricted data sample. Scores are consistently equivalent or better than those achieved by the existing prediction scheme for shear-induced CAT.

Examination of the daily chart products showed variability in the risk areas diagnosed, according to the meteorological conditions, rather than being largely defined by the fixed orography. Thus the use of these forecast fields provides significant added value to the known risk areas.

The use of a single chart to represent the altitude range of upper air forecasts is a limitation to the accuracy of the forecast. However, the savings made on computation and storage are significant when compared to the added effort which would be required to consider a number of height fields in the forecasting environment. The use of gravity wave stress fields only as a diagnostic showed considerable success as a MWT predictor.

The contours displayed were modified during the trial, as it became clear that small areas of particularly high risk were more useful for forecasting MWT than large low risk areas. The use of coloured contours at .0625 Pa and .25 Pa were identified as most useful.

The feedback received from WAFC forecasters throughout the trial period was invaluable in the development of the algorithm into an operationally acceptable tool. The response to the suggested implementation of the product as presented at the end of the trial was very positive, although some concerns have been addressed for future attention.

The combination of subjective, practical and objective assessment of the scheme all showed a strong case for implementation of the algorithm into the forecast tools available to WAFC forecasters.

6 Conclusion and recommendations

This report has documented the development of a prediction scheme for forecasting mountain wave turbulence for civil aviation customers. The regression and other statistical tests described in chapter 4 showed that gravity wave stress fields could be used in the prediction of MWT. The scores from both the initial development and operational trial showed skill for MWT prediction, comparable to that of the existing scheme for shear-induced CAT in the Unified Model. The real time trial project described in chapter 5 was successful in developing the algorithm and its presentation for use in an operational environment.

The use of the gravity wave stress field effectively takes into account the wind and stability conditions required to generate gravity wave activity from the surface and through the atmosphere. Hence, the use of this objective field as a MWT predictor significantly reduces the effort required to diagnose these effects in a pressured forecasting environment.

The results from both the objective verification and forecasters' feedback lead to a recommendation for the implementation of the MWT predictor into the suite of products available to aviation forecasters in the National Meteorological Centre. This new product is intended to complement the existing objective predictor for shear-induced CAT and provide an objective tool for the enhancement of aviation CAT forecasting. These two schemes will contribute to the projected semi-automation of global aviation forecasting.

During the technical implementation of the scheme, care must be taken to retain as much flexibility as possible. The gravity wave drag parameterisation is sensitive to the horizontal resolution of the global model and as such future changes in grid resolution may require amendments to the algorithm. For example, this may involve the inclusion of more gridpoints to represent MWT downstream of the source. The consideration of lower altitudes in the scheme may also require the explicit inclusion of lee wave effects, which here have been discarded for upper tropospheric considerations.

Once the scheme has been implemented into the operational system, the performance and use of the tool should be monitored to identify any systematic limitations. The principle initial concern is that only a single global field is defined and as such no objective height indicator can be used in conjunction with the horizontal extent of the indicated MWT hazard areas. Although the implications of this have been addressed and the need may be small, there may be a future requirement to include additional field(s) to address this issue, or to identify a more empirical method for height estimation.

It is important to monitor not only the objective performance of the predictor, but also its use in the context of the other tools available to the forecasters. Although the final product does not distinguish between sources of CAT, the two CAT predictors must remain separate to avoid confusion to forecasters adding value to the product. It must be made clear that the MWT predictor is an additional tool to enhance current CAT forecasts, while removing the need for time-consuming derivation from surface data.

Finally, to ensure the maximum benefit of the predictor, documentation on the use and limitations of the scheme is required to ensure that forecasters have a full understanding of its scientific derivation and its value in CAT forecasting. This is vital to the future success of this product as a cost-effective enhancement to products supplied to airlines and flight planners worldwide.

References

Bysouth, C.E., 1998: A comparison of clear air turbulence predictors. *UK Met. Office Forecasting Research Technical Report no. 242.*

Doyle, J.D., Shapiro, M.A., Bartels, D., Gall, R, 1998: The numerical simulation and validation of a breaking gravity wave during FASTEX. *16th Conference on Weather Analysis and Forecasting, 11-16 January*. pp 460-462.

Heimann, D., 1997: Mesoscale surface wind characteristics and potential gravity-wave formation during cross-Alpine flow. *Meteorol. Atmos. Phys*, **62**, pp 49-70.

Kim, J., Mahrt, L., 1992; Momentum transport by gravity waves. *Journal of Atmospheric Sciences*. **49**, pp 735-748.

Milton, S.F., Lorrimer, S.J., Chalcroft, B.V., 1998. Parallel trials of enhanced vertical and horizontal resolution in the global Unified Model. *UK Met. Office Forecasting Research Technical Report no. 230.*

Milton, S.F., Wilson, C., Stratton, R.A., Hammon, O., Rawlins, F., 1994: Impact of a new gravity wave drag scheme and orogaraphic roughness in the Unified Model. I. Global model tests. *UK Met. Office Forecasting Research Technical Report no. 127*

Murray, S., Olson, R., 1998: Generation of significant weather forecasts - capabilities at the World Areas Forecast Centres. *8th Conference on Aviation, Range and Space Meteorology, 10-15 January*. pp 90-92.

Shutts, G.J., 1998: Stationary gravity-wave structure in flows with directional wind shear. *Q. J. R. Meteorol. Soc.*, **124**, pp. 1421-1442

Source Book to the Met. Office Forecasters Reference Book. Crown Copyright 1997.

Tilley, J.S., Wilkinson, D.-L., Kelley, H.L., 1998: Short range simulation of an Alaskan clear air turbulence event. *16th Conference on Weather Analysis and Forecasting, 11-16 January*. pp 68-70.

Turner, J.A, Bysouth, C.E., 1998. Automated systems for predicting clear air turbulence in global aviation forecasts. *8th Conference on Aviation, Range and Space Meteorology, 10-15 January*. pp 368-372.

Acknowledgements

Firstly, thanks go the WAFC forecasters who have shown great co-operation and encouragement throughout the winter trial project. I would also like to thank Steve Murray for advice on implementation, and Stuart Webster for valuable discussions and information on model parameterisation aspects.
Finally, a big thank you to my manager Neil Halsey, for his continual support and advice throughout this work.